

# Electron beam physical vapour deposition and mechanical properties of c-ZrO<sub>2</sub>-ZTA-coatings on alloy 617 substrates

E. Roos<sup>a</sup>, S.M. Naga<sup>b,\*</sup>, R.N. Richter<sup>c</sup>, S. Lauf<sup>a</sup>, M. Awaad<sup>b</sup>,  
A. Lyutovich<sup>a</sup>, M.A. Tameem<sup>d</sup>

<sup>a</sup>Materials Testing Institute (MPA), University of Stuttgart, Germany

<sup>b</sup>National Research Centre (NRC), Cairo, Egypt

<sup>c</sup>Fraunhofer Institute for Manufacturing Engineering and Automation IPA, Stuttgart, Germany

<sup>d</sup>MTC, Engineering Mechanics, Cairo, Egypt

Received 21 November 2011; received in revised form 14 December 2011; accepted 15 December 2011

Available online 27 December 2011

## Abstract

Multilayered zirconia toughened alumina (ZTA) and c-zirconia coatings were prepared using electron beam physical vapour deposition (EB-PVD). Characterizations of the morphology and chemical composition of the deposited coatings were performed using scanning electron microscopy (SEM) and X-ray diffraction analysis (XRD). Scratch resistance, nano-indentation and bending strength were used for the evaluation of the mechanical properties. X-ray diffraction of the top ceramic TBC surface showed that it consists entirely of cubic ZrO<sub>2</sub> phase. The energy-dispersive X-ray spectroscopy analysis (EDS) showed that  $\alpha$ -Al<sub>2</sub>O<sub>3</sub> is the only oxide phase present at the interface, while SEM indicated the presence of columnar c-ZrO<sub>2</sub> as the only phase of the top coat. Delamination over a large region was observed in the case of double layer (ZTA) coating. In contrast, the multilayered (ZTA1 + ZTA2 + c-Z) coating showed neither delamination nor cracking. The hardness and scratch measurements showed that the top coat c-ZrO<sub>2</sub> layer is harder than the ZTA layers. The thermal conductivity of the multilayer coatings was estimated using the theoretical density and thermal conductivity values of zirconia toughened alumina (ZTA) and cubic-zirconia (c-ZrO<sub>2</sub>) together with their experimentally measured data.

© 2011 Elsevier Ltd and Techna Group S.r.l. All rights reserved.

**Key words :** C. Hardness; C. Thermal conductivity; Coating; Physical vapour deposition; Scratch

## Introduction

Increasingly stringent demands are being imposed on the efficiency of gas turbine engines employed in the aerospace and power generation industries. The major means for improving turbine efficiency is by increasing operating temperatures in the turbine section of the engines. The materials employed must withstand the higher temperatures as well as mechanical stresses, corrosion, erosion and other severe conditions during operation, while providing extended lifetime as required by the end users.

During the last decade, research efforts were devoted to the development and manufacturing of ceramic thermal barrier coatings (TBCs) on turbine parts because the traditional turbine

materials have reached the limits of their temperature capability. The great advantage of coatings is that it is possible to modify its response to the environment by changing the superficial part of the component, thus providing completely different properties. Thermal barrier coatings (TBCs) are applied for protection of metallic components that suffer degradation due to corrosion, oxidation or excessive heat load during service in thermally drastic environments. TBCs consist typically of a metallic bond coat (MCrAlY where M: Ni, Co, Fe or combination of these elements) and a ceramic top coat normally applied onto a super alloy substrate. Nickel base superalloy with oxidation resistant coating TBC were acknowledged as a standard material system for turbine engineering in the near future (next 15 years and longer) [1]. It is important to mention that the durability of the MCrAlY coating depends not only on coatings composition, but also on the surface engineering technique.

\* Corresponding author at: National Research Center, Ceramics Department, Cairo, Egypt. Tel.: +20 233337143; fax: +20 233370931.

E-mail address: [salmanaga@yahoo.com](mailto:salmanaga@yahoo.com) (S.M. Naga).

Ceramic coatings have been applied by several methods: sputtering, air plasma spray (APS) and electron beam-physical vapour deposition (EB-PVD). EB-PVD has the advantage of using a focused high-power electron beam, which melts and evaporates metals as well as ceramics. Electron beam-physical vapour deposited TBCs are used on the hot section of aircraft turbines to extend the life of metal components [2].

Among the TBCs, APS and EB-PVD, yttria-stabilized zirconia TBCs have been widely studied because of (in part) their low thermal conductivity, their good match to the thermal expansion coefficient ( $\approx 10\text{--}5\text{ K}^{-1}$ ) of Ni-based super alloys, and their acceptable durability during thermal cycling [3–6]. EB-PVD-TBCs have recently received attention because the coatings are expected to surpass APS-TBCs in mechanical performance [7]. The EB-PVD process is known to be reliable and strain-tolerant because it can produce TBCs with a unique columnar microstructure at high deposition rates, and can form durable and dense layers containing nano-sized pores, nano-gaps and some feather-like structures [8–10]. Kwon et al. [10] indicated that a thick bond coat is more efficient for protecting the substrate from the contact environment than thin bond coat. They showed that TBC systems without top coat, i.e. bond coat/substrate system, exhibits well-defined damage within the bond coat, with a minor damage in the substrate. The damage formed in the thick bond coat is not extended and the bond coat/substrate only shows damage that has accumulated within the bond coat at relatively low load, whereas the damage zone in the thin bond coat is well defined in the substrate. Bouzakis et al. [11] stated that in order to avoid apparent creep phenomenon and subsequent  $\text{ZrO}_2$  coating failure of EB-PVD-TBCs, the optimal maximum equivalent stress at which TBC can operate has to be less than its corresponding critical stress value. Johnson et al. [12] studied the relationship between residual stress, microstructure and mechanical properties of EB-PVD-TBCs. They showed that the strain tolerance of the coating decreased with increasing residual stress.

Further improvements can be introduced using intermediate layers considering the chemical affinity between the ceramic top layer and metallic substrate (material adapter) [13], with optimization of ceramic materials or to alter the chosen ceramic materials with lower thermal conductivity, which can be achieved by control of the pores, whose formation are dependent on the coating process parameters.

In the present investigation, 15 mol% zirconia toughened alumina (15-ZTA) is used as the diffusion barrier layer, oxidation protective layer and as well as material adapter for c- $\text{ZrO}_2$  as the ceramic top coat.  $\text{Al}_2\text{O}_3$  replace conventionally used expensive  $\text{Y}_2\text{O}_3$ .

## 1. Experimental

### 1.1. Materials

#### 1.1.1. Preparation of the starting materials

The materials used for this investigation were zirconium n-(IV) butoxide (Strem chemicals, Newburyport MA, USA),

aluminium tri-isopropoxide (Merck, Germany) and  $\text{Y}_2\text{O}_3$  powder (99.99%, Strem chemicals, Newburyport MA, USA). Alumina and zirconia toughened alumina were prepared and mixed according to the procedures mentioned elsewhere [13].

#### 1.1.2. Preparation of EB-PVD targets

Conical targets were formed by casting technique. The targets were dried at  $110^\circ\text{C}$  and sintered at  $1650^\circ\text{C}$  to give as high-density cones as possible for EB-PVD deposition.

### 1.2. Electron beam physical vapour deposition (EB-PVD)

ZTA-15 and cubic zirconia-coatings were deposited by electron beam evaporation on 617-nickel based superalloy substrates [13].

Squared samples were used for optical and scanning electron microscopy (top view and cross section), micro-hardness and scratch testing characterization. For bending strength testing, rectangular bars ( $60\text{ mm} \times 5\text{ mm} \times 3\text{ mm}$ ) were used.

Both substrates were first coated with two successive 15 mol% ZTA layers. On these layers, one layer of c- $\text{ZrO}_2$  is deposited. Fig. 1 shows a schematic representation of multi-layered coatings obtained by EB-PVD technique. The layers are denoted as follows: first zirconia toughened alumina layer (ZTA1), first and second zirconia toughened alumina layer (ZTA2), and the final coat containing zirconia toughened alumina layers + c-zirconia (c-Z).

## 2. Characterization

### 2.1. Phase composition and microstructure evolution

XRD analysis (Philips 1730 diffractometer, Netherlands) with a Ni-filtered and monochromated  $\text{Cu K}\alpha$  radiation with goniometric range  $10\text{--}80$  and scan speed of  $18/\text{min.}$ , was applied to identify crystalline phases of the coatings. Care was taken to maintain the current at 40 kV and 40 mA during the experiment.

The morphology of the films was studied using optical microscopy (Jeol, OM), and scanning electron microscopy (Jeol). The distribution of the elements in the system coatings/interface/substrate was measured using line-scan EDS on the cross-sections of the samples. The top coat is analysed by XRD to detect the formed phase of zirconia.

The average pore size and pore-size distribution of the sintered bodies were obtained using high pressure mercury porosimetry (Model 200 porosimeter, Carlo Erba, Milan, Italy).

### 2.2. Mechanical properties

#### 2.2.1. Bending-test

The three point bend strength of the fired samples was determined using specimens of diameters  $6\text{ mm} \times 3\text{ mm} \times 50\text{ mm}$  and a universal testing machine Model (MTS Sintech

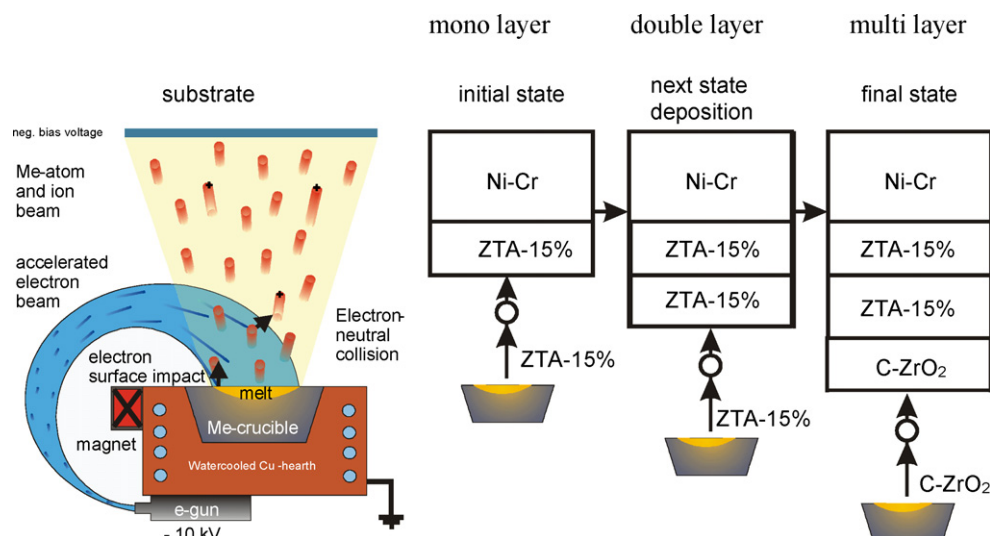


Fig. 1. Scheme of the multilayer coating.

65/G). The span width of the bearing rollers was 28 mm and the central loading roller is fixed within a traverse guided by ball-type nipples.

Due to the compliance of the arrangement within the loading frame the bending was directly measured by using a transducer (LVDT) with high resolution. To optimize the arrangement and for purposes of comparison, two uncoated specimen were tested up to the inelastic region.

Based on this result the further tests were improved by conducting a stepwise loading at 50 N, 120 N, 300 N, 500 N, 600 N, 700 N and 800 N each with complete unloading followed by optical microscopy to detect possible failures.

#### 2.2.2. Nano-scratch test

The nano-scratch test (NST) provides detailed information about the generation of a single scratch. It is used for the characterization of organic coatings [14–16] as well as Polymers and hard coatings [17]. An indenter of Rockwell geometry (conical, die angle  $90^\circ$ , tip radius  $2\ \mu\text{m}$ ) is pushed with increasing load (80 mN/min) into the sample, which is moved with a constant velocity (in this case 3 mm/min). During the scratch process data of the tangential  $F_t$  and the normal force  $F_n$  as well as the depth are recorded. The penetration depth  $d_p$  of the indenter and the remaining depth of the scratch (residual depth  $d_r$ ) are calculated using the data of a surface scan with minimal load before (pre-scan) and after (posts-can) the scratch

#### 2.2.3. Indentation hardness

Indentation hardness was measured using a Fischerscope HM 2000 (Helmut Fischer GmbH+ Co. KG, Sindelfingen) equipped with a Vickers diamond. To get depth resolved hardness values the ESP (Enhanced Stiffness Procedure) [18] mode was used. In this mode the loading is periodically interrupted by an unloading cycle to determine depth resolved values of EIT and HM according to DIN\_EN\_ISO\_14577-1 within one indentation.

### 3. Results and discussion

#### 3.1. Phase composition and microstructure evolution

X-ray diffraction of the top ceramic TBC surface shows that it is composed entirely of cubic  $\text{ZrO}_2$  phase (Fig. 2).

The multilayer nature of the ceramic TBC formed by EB-PVD is illustrated in Fig. 3. The EB-PVD ceramic coating has a unique columnar morphology. The columnar grains grow perpendicular to the substrate surface and extend through the entire c- $\text{ZrO}_2$  ceramic coating thickness.

Fig. 4 shows the detailed chemical analysis of each layer of the coat. The figure indicates the formation of an interface zone (Fig. 4, spectrum 2). The composition and microstructure of that zone strongly depends on the type and microstructure of the phases present on top of the coat before YSZ deposition. The EDS analysis shows that the thermodynamically  $\alpha\text{-Al}_2\text{O}_3$  is the only oxide phase present at the interface. The most assumed

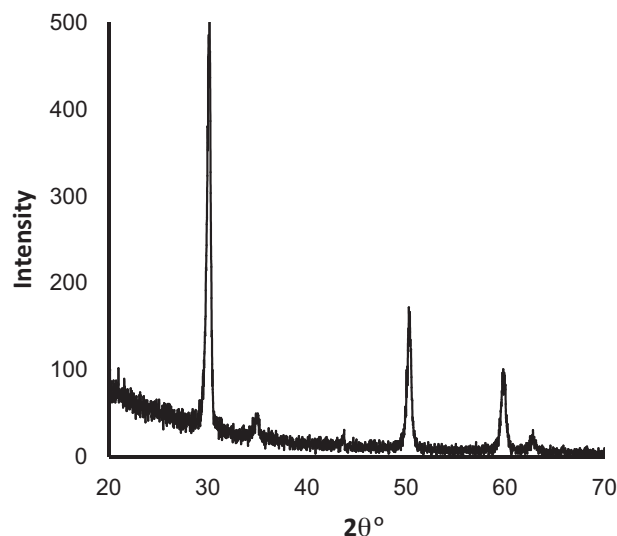


Fig. 2. XRD patterns of the top ceramic TBC surface.

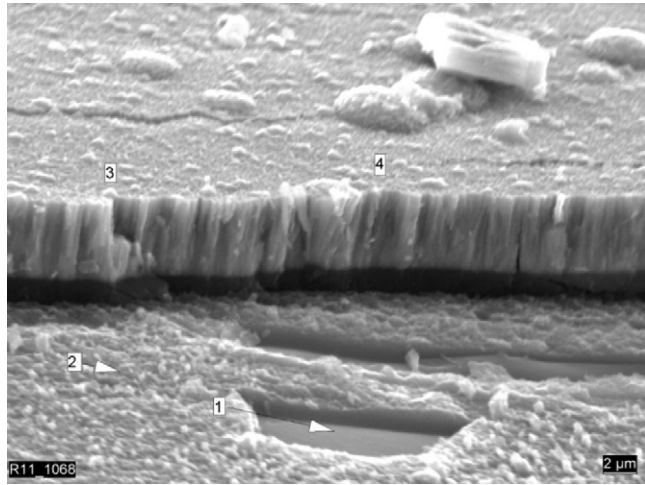


Fig. 3. SEM micrograph of the TBC multilayer.

scenario for the formation of that interface zone is the deposition of thick theta alumina on the  $\beta$ -NiAl phase in MCrAlY's [19]. Mixed zones have been identified for platinized NiCoCrAlY bond coat that form substantial amounts of theta alumina [20]. They have, also been detected for CoNiCrAlY/EB-PVD YSZ TBC systems after manufacture [21]. In these observations only  $\alpha$ -Al<sub>2</sub>O<sub>3</sub> has been detected. The current results validate the observations on formation of an interface zone on EB-PVD NiCoCrAlY coat systems. Spectrum 1 represents the typical chemical analysis of the Ni based alloys. On the other hand, the region between the interface and the columnar c-ZrO<sub>2</sub> structure indicates the presence of Al<sub>2</sub>O<sub>3</sub> and ZrO<sub>2</sub>. The chemical analysis of the columnar microstructure shows that it composed of only c-ZrO<sub>2</sub> phase (Fig. 4, spectra 3 and 4).

### 3.2. Physical properties

Table 1 illustrates the porosity, pore diameter and pore volume of the multilayer coat. It shows that the porosity and total pore area increase in the top layer in comparison to the ZTA1 and ZTA2. Zirconia toughened alumina coats (ZTA1 and ZTA2) show the same porosity figures. On the other hand, c-ZrO<sub>2</sub> coat layer shows an increase in the total porosity values.

### 3.3. Calculated thermal conductivity

The studied multilayer coating was investigated to get the overall thermal conductivity. The case studied here is a combination between conduction and convection. The conduction took place through the dense materials either zirconia toughened alumina or c-zirconia, keeping in mind the effect of the material porosity, as the porosity affects negatively the thermal conductivity. The other mechanism in heat conduction presented here is the heat transfer which took place in the interface between different coating layers. The heat transfer coefficient between different layers  $h_i$  tends to be infinity in perfect bonding between layers which means no temperature drop due to bonding imperfection while  $h_i$  value decrease as

imperfections and delamination between layers increase and so temperature drop occurs, according to the following equation [22]:

$$Q = h_i A \Delta T \quad (1)$$

where,  $\Delta T$  is the temperature drop;  $Q$  is the heat flux through such an interface;  $h_i$ , is thermal conductivity coefficient;  $A$  is the normal areal where the heat pass through.

According to Ravichandran and An [22] the thermal conductivity of the composite coating is given by the following equation.

$$k_{mc} = \frac{L_m}{n_{al} L_a / k_{al}^* + n_{zl} L_z / k_{zl}^* + (n_{al} + n_{zl} - 1) / h_{il}} \quad (2)$$

where  $L_m$  is the total thickness of the multilayer coating,  $n_{al}$  and  $n_{zl}$  are the number of Al<sub>2</sub>O<sub>3</sub> and c-ZrO<sub>2</sub> layers, respectively,  $L_a$  and  $L_z$  are the thicknesses of the Al<sub>2</sub>O<sub>3</sub> and c-ZrO<sub>2</sub> layers, respectively, and  $h_{il}$  is the heat-transfer coefficient for the interlayer interface between Al<sub>2</sub>O<sub>3</sub> and c-ZrO<sub>2</sub>. The parameters  $k_{al}^*$  and  $k_{zl}^*$  are the effective thermal conductivities of the Al<sub>2</sub>O<sub>3</sub> and c-ZrO<sub>2</sub> layers, respectively; these parameters incorporate the influence of porosity and the resistance to heat transfer across the interfaces between the splats in each material. A simple relationship to describe the thermal conductivity of two-phase materials was deduced [21] on the basis of a unit cell model of the microstructure. Using the following relationships,  $k_{al}^*$  and  $k_{zl}^*$  can be calculated:

$$k_{al}^* = k_{al} (1 - p_a^{2/3}) \quad (3)$$

$$k_{zl}^* = k_{zl} (1 - p_z^{2/3}) \quad (4)$$

where,  $p_a$  and  $p_z$  are the volume fractions of porosity in the respective Al<sub>2</sub>O<sub>3</sub> and c-ZrO<sub>2</sub> layers. The parameters  $k_{al}$  and  $k_{zl}$  are the thermal conductivity levels of the Al<sub>2</sub>O<sub>3</sub> and c-ZrO<sub>2</sub> layers, respectively; these parameters also incorporate the thermal resistance due to splat interfaces that are present in each layer.

Based on the theoretical density and thermal conductivity data of zirconia toughened alumina (ZTA) and cubic-zirconia (c-ZrO<sub>2</sub>), and the data given in Table 1 and Fig. 3 the thermal conductivity coefficient was calculated. The thermal conductivity coefficient ( $h_i$ ) of the studied multilayer was estimated by applying Eqs. (2)–(5). It was found to be 1000 W/(m K). According to the imperfection in bonding between the coating layers (as the value of  $h_i$  increases this indicates that no temperature drop across the coating layers and vice versa),  $h_i$  tends to be  $\infty$  in perfect layer bonding. The calculated overall thermal conductivity from room temperature to 1000 °C was 2.55 W/(m K). It is interesting to note that experimentally measured thermal conductivity of 8 YSZ is 2.3 W/(m K), while the theoretically predicted value is 3.2 W/(m K) [23]. Raghavan et al. [24] stated in their study that the thermal conductivity of 20 Y (Ta or Nb) O<sub>4</sub> doped zirconia is similar to that seen in commonly used 4.2 mol% YSZ.

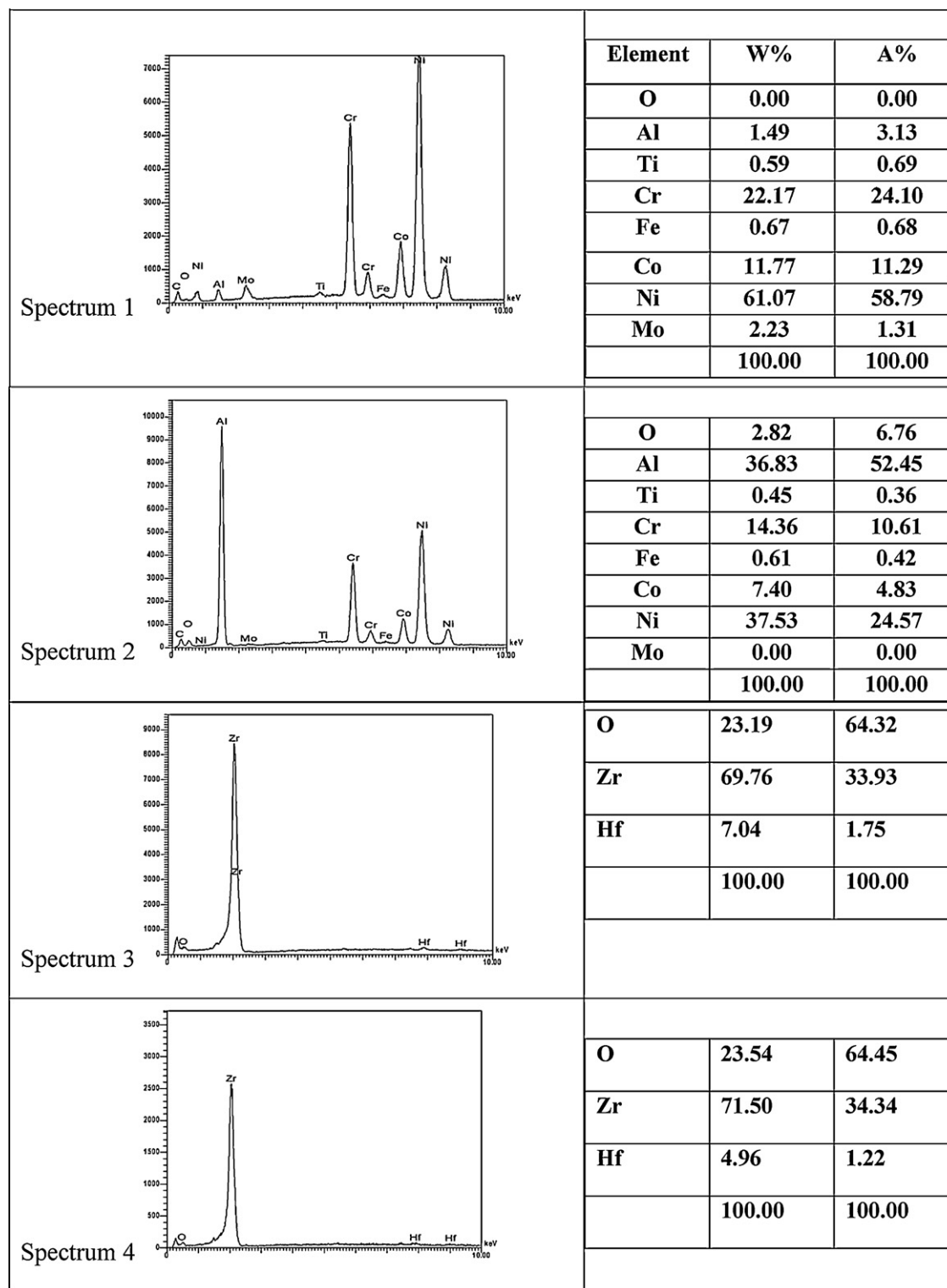


Fig. 4. EDS and chemical composition of the deposited multilayer.

Table 1

Studied multilayer coat porosity, total pore area and average pore diameter.

Layer	Total intrusion volume, ml/g	Total pore area, m <sup>2</sup> /g	Av. pore diameter, μm	Total Porosity, %
ZTA1 (single layer)	0.0015	0.498	0.0117	1.34
ZTA2 (double layer)	0.0015	0.498	0.0117	1.35
c-ZrO <sub>2</sub> (multilayer)	0.0042	1.513	0.0112	2.75



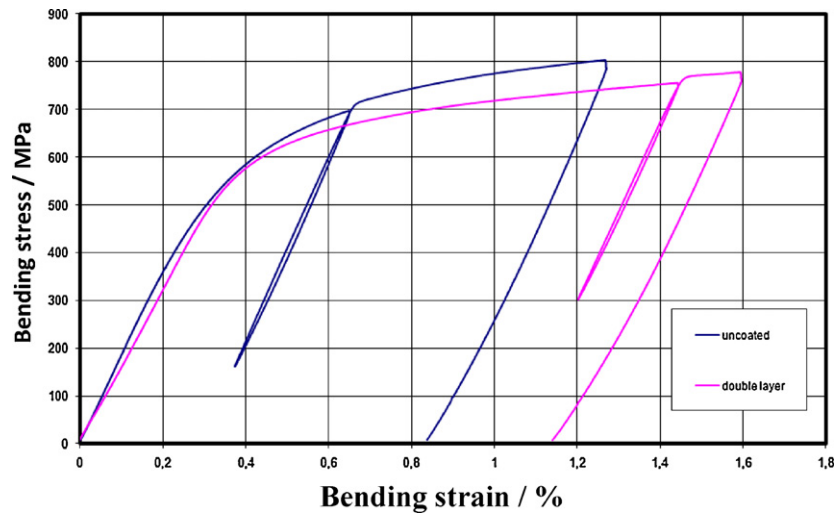


Fig. 5. Stress–strain behaviour of uncoated and double layer coated specimen under bending loading.

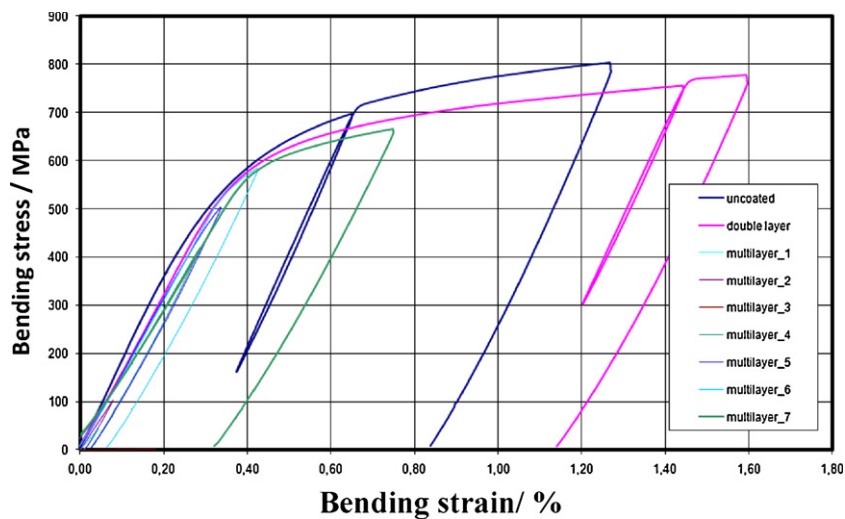


Fig. 6. Stress–strain behaviour of double layer and multi layer specimens under bending loading.

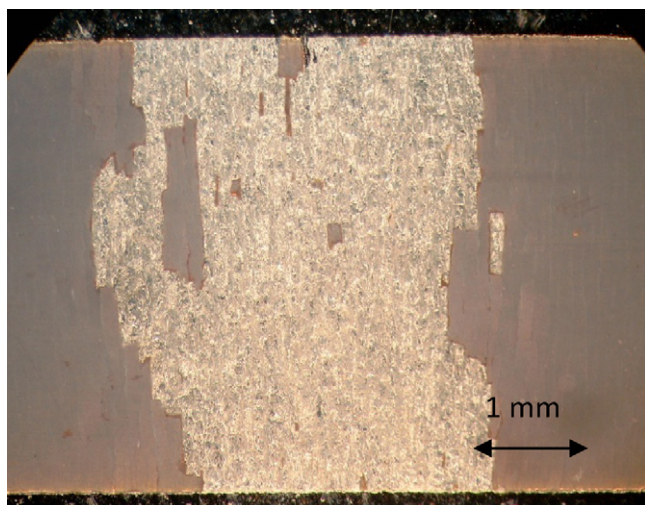


Fig. 7. Delamination of double layer.

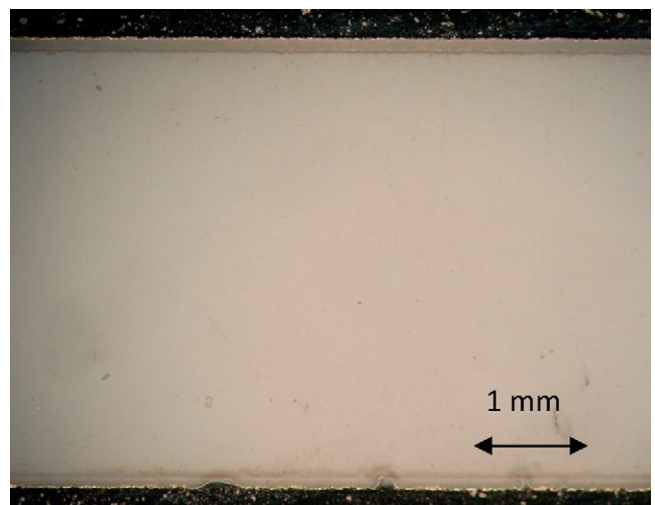


Fig. 8. Undamaged multi layer.

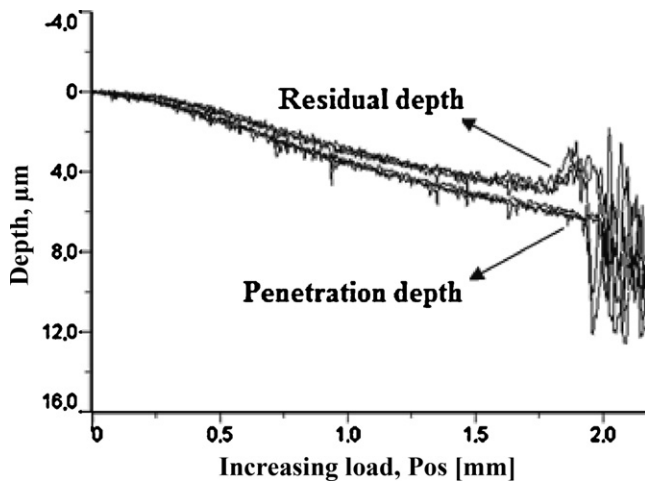


Fig. 9. Penetration depth (down curve) and residual depth (up curve) during scratch test with increasing load (double layer).

### 3.4. Mechanical properties

#### 3.4.1. Bending strength

All tests were performed with partial unloading after reaching the inelastic region. Bending was in the range of component relevant stresses far below the fracture strength. According to the very thin coating no pop ins of loading were observed (Figs. 5 and 6).

Using optical microscopy (Leica MZ6) double layered specimen shows the delamination of the coating over a large region.

In contrary to the double layered specimen the multi layered specimen didn't show any delamination or cracking (Figs. 7 and 8). This comparison is not final because the maximum strain was chosen lower.

The results show that three-point-bending may be used for integral measurement of adhesion of layers. For quantitative analysis of adhesion especially at double layers the scratch test should be used. More subtle methods like nano-indentation and acoustic emission may improve the analysis.

#### 3.4.2. Nano-scratch test

Fig. 9 shows the penetration depth ( $d_p$ ) and residual depth ( $d_r$ ) of the double layer sample, the other samples showed similar results. After a smooth part the curve shows rapid fluctuations at a penetration depth of about 5  $\mu\text{m}$ . This indicates a mechanical failure of the material. The maximum depth of  $p_d$  is about 12  $\mu\text{m}$ . Optical micrographs of the scratch groove (Fig. 10) show that in the beginning of the scratch the trace almost vanishes within the surface roughness. The increasing normal force forms a smooth scratch groove, but at a certain force the surface cracks. This critical force is characteristic for the material and the layer thickness.

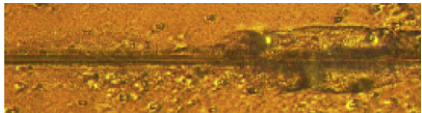
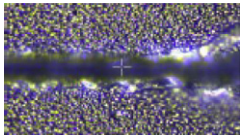
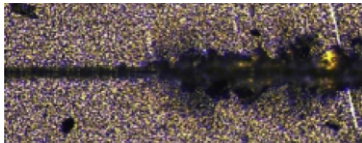
Table 2 summarizes the critical loads, the corresponding penetration depth and a microscopical image. The penetration depth indicates the layer where the failure occurs. The multi layer cracks at a depth of 1.5  $\mu\text{m}$ , which matches with the thickness of the c-ZrO<sub>2</sub> layer. The double layer cracks at 6  $\mu\text{m}$  respectively 7.5  $\mu\text{m}$  which is equal to the total coating thickness. The brittle failure occurs at reaching the coating/substrate interface.

The prescan provides a surface profile from which roughness parameters can be evaluated. According to DIN EN ISO 8503-1 the characteristics  $R_z$  (average distance between highest peak and lowest valley within a sample length),  $R_{\text{max}}$  (maximum of  $R_z$  values within total measured profile) and  $R_a$  (arithmetic average of the distance to the centre line) were calculated using a Gauss filter with  $\lambda_c = 0.25$  mm and are shown in Table 3.

#### 3.4.3. Hardness

**3.4.3.1. Vickers microhardness (HV0.1).** The Vickers microhardness values, HV0.1, of the double and multilayer in the TBC system are shown in Fig. 11. The results show an increase of the microhardness on passing from the double layer to the top coat. The cracking or delamination at the interface between ZTA coat and the top coat (Fig. 10), will be expected to occur in the indentation tests as the differences in the values of HV0.1 increases, because of the elastic/plastic mismatch stress present [25].

Table 2  
Critical loads and corresponding penetration depth and image of the point of failure.

Layer	Critical load (mN)	Penetration depth ( $\mu\text{m}$ )	Image
Multi layer	83	1.5	
Single layer	42	6.0	
Double layer	79	7.5	

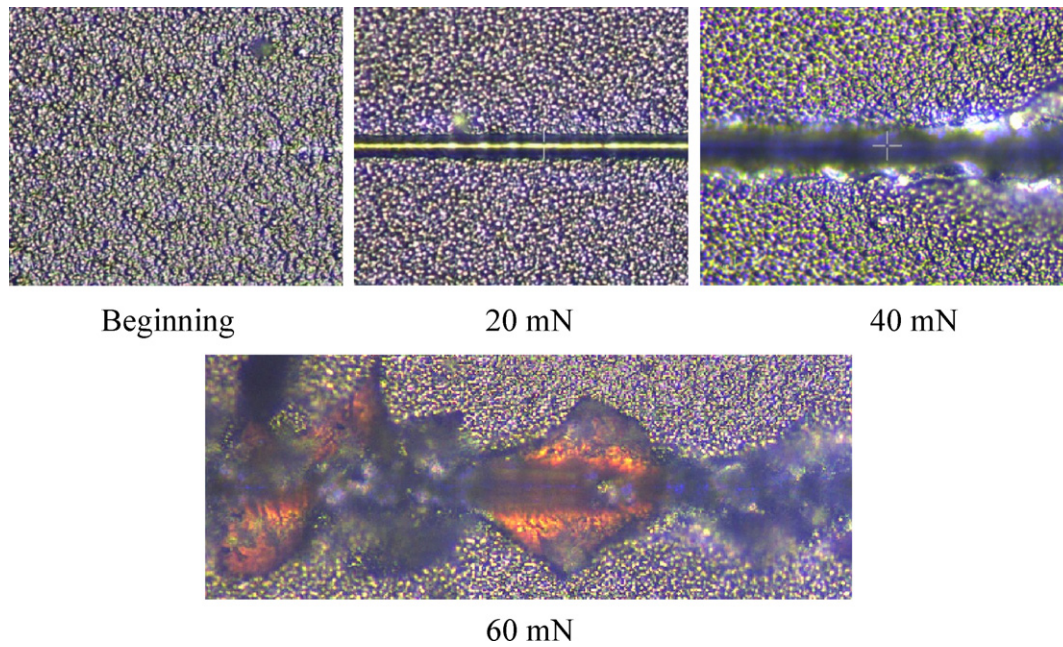


Fig. 10. Optical micrographs of the scratch groove at different normal forces, double layer.

Table 3  
Roughness parameters of the different layers.

Material	$R_z$ [ $\mu\text{m}$ ]	$R_{\text{max}}$ [ $\mu\text{m}$ ]	$R_a$ [ $\mu\text{m}$ ]
Multilayer	0.68	1.13	0.073
Double layer	0.34	0.54	0.033

**3.4.3.2. Martens microhardness (HM).** Fig. 12 shows the load-depth curves of a double layer sample. The spikes pointing to the left show the unloading cycles during indentation. Reduced Young's Modulus  $E_{\text{IT}}$  and the Martens hardness  $H_M$  were calculated according to DIN\_EN\_ISO\_14577-1 within the same indentation.

The depth resolved hardness measurement showed that the ZTA double layer is much softer than the multi layer (Fig. 13). Both samples of ZTA double layer (blue curves) show a good

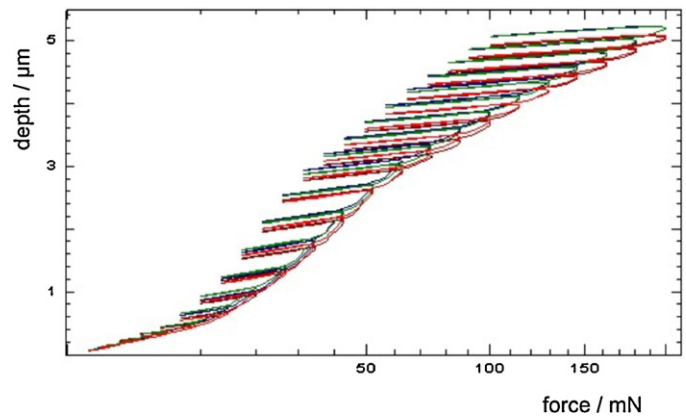


Fig. 12. Load-depth curves in ESP-mode of the double layer sample; the three curves show the excellent reproducibility.

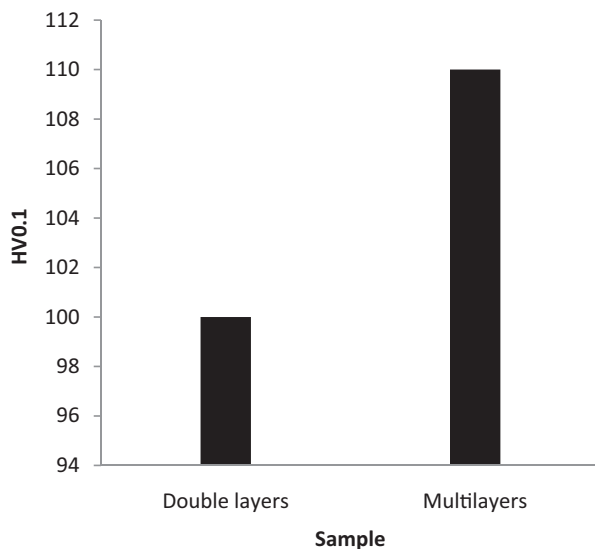


Fig. 11. Studied samples microhardness (substrate, ZTA, c-ZrO<sub>2</sub>).

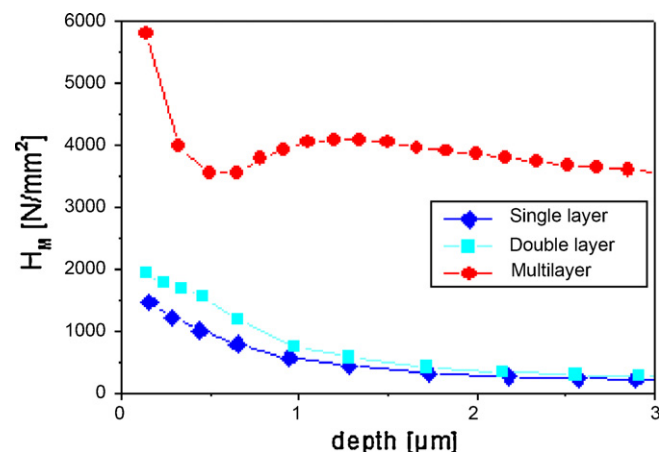


Fig. 13. Martens hardness as function of penetration depth.



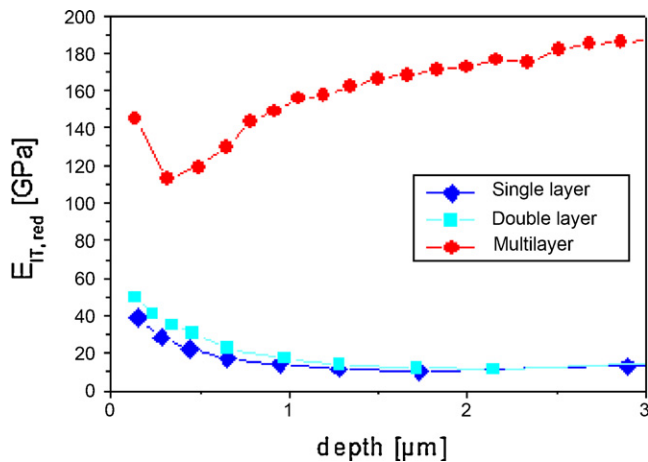


Fig. 14. Young's modulus as function of penetration depth.

reproducibility. The decay of the hardness curves of ZTA indicates that the substrate is softer than the ZTA. Hardness stays constant above a depth of 2  $\mu\text{m}$ .

The multi layer sample shows a minimum in hardness at 0.5  $\mu\text{m}$  depth. This is due to the influence of the softer ZTA layers below the c-ZrO<sub>2</sub> layer, which starts after penetrating about 10% of that layer [17]. The hardness increases again and reaches a maximum at 1.2  $\mu\text{m}$  penetration depth, which coincides with the critical depth of the NST experiment (Table 3). The curves are mean values out of three measurements.

Fig. 14 shows the reduced Young's modulus as a function of penetration depth. c-ZrO<sub>2</sub> layer has higher Young's modulus than the ZTA layers with analogous behaviour to the hardness. The minimum of the modulus curve occurs at a lower depth than the hardness curve. The Young's modulus rises again above a penetration depth of 1.7  $\mu\text{m}$ . This indicates that the modulus of the substrate is higher than the coated layers.

#### 4. Conclusions

1. The EB-PVD ceramic coating has a unique columnar morphology. The columnar grains grow perpendicular to the substrate surface and extend through the entire c-ZrO<sub>2</sub> ceramic coating thickness.
2. The current results indicate the formation of an interface zone on EB-PVD NiCoCrAlY coat system.
3. Based on the theoretically dense zirconia toughened alumina and c-zirconia, thermal conductivity and porosity data of the studied material and its multilayer thickness the thermal conductivity coefficient ( $h_i$ ) of the studied multilayer material was estimated to be = 1000 W/(m K).
4. The Vickers microhardness results show a step-like decrease on passing from the substrate to the top coat.
5. The depth resolved hardness measurement showed that the ZTA layers are much softer than the coating layer.

#### References

[1] E. Roos, K. Maile, A. Lyutovich, Materials for advanced power engineering, in: J. Lecomte-Beckers, Q. Contrepolis, T. Beck, B. Kuhn (Eds.), Proceedings of the 9th Liege Conference, 2010, pp. 660–667.

[2] D.V. Rigney, R. Viguie, D.J. Wortman, D.W. Skelly, PVD thermal barrier coating applications and process development for aircraft engines, *J. Thermal Spray Technol.* 6 (1997) 167.

[3] M. Peters, C. Leyens, U. Schulz, W.A. Kaysser, EB-PVD thermal barrier coatings for aeroengines and gas turbines, *Adv. Eng. Mater.* 3 (4) (2001) 193–204.

[4] N.P. Padture, M. Geell, E.H. Jordan, Thermal barrier coatings for gas-turbine engine applications, *Science* 296 (2002) 280–284.

[5] W. Beele, G. Marijnissen, A. van Lieshout, The evolution of thermal barrier coatings-status and upcoming solutions for today's key issues, *Surf. Coat. Technol.* 120–121 (1999) 61–67.

[6] E. Tzimas, H. Mullojans, S.D. Peteves, J. Bressers, W. Stamm, Failure of thermal barrier coating systems under cyclic thermomechanical loading, *Acta Mater.* 48 (2000) 4699–4707.

[7] S. Guo, Y. Tanaka, Y. Kagawa, Effect of interface roughness and coating thickness on interfacial shear mechanical properties of EB-PVD yttria – partially stabilized zirconia thermal barrier coating systems, *J. Eur. Ceram. Soc.* 27 (2007) 3425–3431.

[8] B.K. Jang, H. Matsubara, Influence of porosity on hardness and Young's modulus of nanoporous EB-PVD-TBCs by nanoindentation, *Mater. Lett.* 59 (2005) 3462–3466.

[9] U. Schulz, K. Fritscher, A.E. Stahl, Cyclic behaviour of EB-PVD thermal barrier coating systems with modified bond coats, *Surf. Coat. Technol.* 203 (2008) 449–455.

[10] J.-Y. Kwon, J.-Lee, Y.-G. Jung, U. Paik, Effect of bond coat nature and thickness on mechanical characteristic and contact damage of zirconia-based thermal barrier coatings, *Surf. Coat. Technol.* 201 (2006) 3483–3490.

[11] K.-D. Bouzakis, A. Lontos, M. Michailidid, O. Knotek, E. Lugscheider, K. Bobzin, A. Etzkorn, Determination of mechanical properties of electron beam – physical vapour deposition – thermal barrier coatings (EB-PVD-TBCs) by means of nanoindentation and impact testing, *Surf. Coat. Technol.* 163–164 (163) (2003) 75–80.

[12] C.A. Johnson, K.A. Ruud, R. Bruce, D. Wortman, Relationships between residual stress, microstructure and mechanical properties of electron beam – physical vapour deposition – thermal barrier coatings, *Surf. Coat. Technol.* 108–109 (1998) 80–85.

[13] S.M. Naga, S.H. Kenawy, M.A. waad, E. Roos, A. Lyutovich, H. Ruoff, R. Krisch, Combined zirconia toughened alumina (ZTA) stacks obtained by electron beam physical vapour deposition, *Ceram. Int.* 37 (2011) 771–777.

[14] R.N. Richter, D. Koch, T. Schauer, T. Klimmasch, Insights into the effectiveness of scratch resistant coatings, in: Proceedings of European Coatings Conference, 2009.

[15] R. Nothhelfer-Richter, E. Klinke, C.D. Eisenbach, Neue Erkenntnisse über die Kratzfestigkeit von Klarlacken aus dem Nano-Scratch-Test unter trockenen und nassen Bedingungen, *Farbe u. Lack.* 111 (12) (2005) 42–46.

[16] R.N. Richter, E. Klinke, C.D. Eisenbach, *Proc. Macromol. Symp.* 187 (2002) 853–860.

[17] J. Nohava, Characterization of Thermal Spray Coatings by Instrumented Indentation and Scratch Testing, CSM Instruments Inc., 2009 Online application bulletin no. 28 located at <http://www.csm-instruments.com/en/CSM-Applications-Bulletins>.

[18] Gottfried Bosch, Enhanced Stiffness Procedure mit dem Messgerät Fischerscope HM2000 und Picodentor HM500, [http://www.helmut-fischer.com/globalfiles/DE\\_ESP%20Applikationsbericht\\_DE.pdf](http://www.helmut-fischer.com/globalfiles/DE_ESP%20Applikationsbericht_DE.pdf).

[19] R.M. Arroyo, D. Clemens, F. Tietz, R. Anton, J. Quadackers, L. Singheiser, Influence of composition and phase distribution on the oxidation behaviour of NiCoCrAlY alloys, *High Temp. Corros. Prot. Mater.* 5 (369–372) (2001) 165–172.

[20] W.J. Quadackers, V. Shemet, D. Sebold, R. Anton, E. Wesel, L. Singheiser, Oxidation characteristics of a platinised MCrAlY bond coat for TBC systems during cyclic oxidation at 1000 °C, *Surf. Coat. Technol.* 199 (2005) 77–82.

[21] A.J. Burns, R. Subramanian, B.W. Kempshall, Y.H. Sohn, Microstructure of as – coated thermal barrier coating with varying lifetimes, *Surf. Coat. Technol.* 177–178 (2004) 89–96.

- [22] K.S. Ravichandran, K. An, Thermal conductivity of plasma-sprayed monolithic and multilayer coatings of alumina and yttria-stabilized zirconia, *J. Am. Ceram. Soc.* 82 (3) (1999) 673–682.
- [23] S. Raghavan, H. Wang, R.B. Dinwiddie, W.D. Porter, M.J. Mayo, The effect of grain size, porosity and yttria content on the thermal conductivity of nano crystalline zirconia, *Scr. Mater.* 39 (8) (1998) 1119–1125.
- [24] S. Raghavan, H. Wang, R.B. Dinwiddie, W.D. Porter, M.J. Mayo, Thermal properties of zirconia co-doped with trivalent and pentavalent oxides, *Acta Mater.* 49 (2001) 169–179.
- [25] H.J. Jang, D.H. Park, Y.G. Jung, J.C. Jang, S.C. Choi, U. Paik, Mechanical characterization and thermal behaviour of HVOF – sprayed bond coat in thermal barrier coatings (TBCs), *Surf. Coat. Technol.* 200 (14,15) (2006) 4355–4362.